DIELECTRIC BEHAVIOR AND PTCR AFFECT IN NANO-CRYSTALLITE PT FERROELECTRIC CERAMICS

I. KASHIF[1], SAMY A. RAHMAN[2], E. M. IBRAHIM[3], A. ABDELGHANY[4] & R. EL-SAID[5]

[1]Department of Physics, Faculty of Science, Al-Azhar University, Cairo, Egypt

[2,3]Department of Physics and Mathematical Engineering, Faculty of Engineering, Ain-Shams University, Cairo, Egypt

[4,5]Department of Physics, Faculty of Science (Girls), Al-Azhar University, Cairo, Egypt

ABSTRACT

The AC behavior of the nano-crystallite PT ceramic sample was studied in wide temperature and frequency ranges. The results show diffuse phase transition and a positive temperature coefficient of resistivity (PTCR) was observed in the temperature dependence of the ceramic resistivity. The results are explained based on the Heywang and Jonker models. The Schottky barrier formed at grain boundary regions act as traps of the electrons available from oxygen vacancies in the ceramics. This provides PTCR characteristics from the transition temperature to about 210°C. A separation of the grain and grain boundary properties has been achieved using equivalent circuit model in impedance analysis.

KEYWORDS: Nano-Crystallite PT Ceramic, AC Properties, Positive Temperature Coefficient of Resistivity (PTCR)

INTRODUCTION

Lead titanate (PT) is a potentially useful ferroelectric material, which shows high electromechanical anisotropy in the piezoelectric response [1, 2].

It is well known that the doped barium titanate ceramics exhibit an anomalous increase in resistivity by 3 to 7 order of magnitude near the ferroelectric transition temperature. This phenomenon is commonly known as positive temperature coefficient of resistivity (PTCR) [3-6].

The PTCR effect has many technological applications as thermal fuses, thermistors, soft circuits and other overload protection devices [4, 5]. The PTCR effect is also observed in several other ferroelectric materials like $KNbO_3$, $NaBiTi_2O_6$ and $KBiTi_2O_6$ [7, 8].

Positive temperature coefficient of resistance (PTCR) characteristic involves a substantial non-linear change of resistivity with temperature around the Curie temperature (Tc) [9–19]. Several models have been developed to explain the PTCR characteristics [10, 11, 13, and 15]. One of the most recognized theories to explain the PTCR characteristics is the Heywang's model [10, 13]. The model is based on the formation of a potential barrier at the grain boundaries.

This model has been extending by Jonker [11], who took into account the influence of the polarization on the resistivity below the Curie temperature. This model is termed the Heywang–Jonker model. This PTCR characteristic has found wide applications as color TV degausser, motor starter, self-regulating heaters, over current limiters and so on [16].

In the present work, we study the AC behavior and PTCR effect in nano-crystallite lead titanate.

Experimental Work

Lead titanate, $PbTiO_3$ (i.e. PT) powders were prepared using a solid-state reaction method. The starting oxides that were used to form the system of samples were as follow: PbO and TiO_2 with purity 99.999 as raw materials in a stoichiometric amount to synthesize. These oxides was mixed and milled in a milling speedball mill type MLW Km1. The precursor powders were then calcined accordingly at 950o C for 4 hours.

The calcined powder was crushed and milled again and sintered at 850 ^{o}C for 2 hours to produce PT phases. After that, phase characterization of the PT powders was carried out by room temperature X-ray diffraction (XRD; PhilipsPW1729 diffractometer) using Ni-filtered Cu Kα radiation. Electrodes were fabricated on the parallel faces of the ceramic disk (9.8 mm of diameter and 1.8 mm of thickness) by using Ag strips and a silver paste. The AC response was studied from 100 Hz to 100 KHz by using programmable RLC Bridge (Philips PM6304). A wide temperature range was analyzed from room temperature (18 ^{o}C) to 500 ^{o}C.

RESULTS AND DISCUSSIONS

The average crystallite size may be calculated by using Scherer equation [20]:

$$D = k\lambda /\beta \cos\theta \tag{1}$$

Where K is a shape factor (0.9- 1), D is the crystallite size in nm, λ is the wavelength of the used X-ray, β is the full width of the diffracted line measured at half its maximum intensity in radians and θ is the angle of diffraction of the top of the peak.

Also the average crystallite size calculated by (win-fit) program [21], from results obtained by (win-fit) program can be note that the two results are in good agreement and equal 59.04 nm. Such size values classify the studied samples as nanocrystalline materials [22]. Also the mean lattice distortion or lattice strain can be calculated by using formula

$$e= \beta/4\tan \theta \tag{2}$$

and equal 2.159×10^{-3}

The density of sample can be calculated by using the relation

$$d= 1/ \Sigma(a_i/d_i) \tag{3}$$

where a_i is the weight fraction of the oxides used in preparing the sample, d_i is the density of these oxides forming the sample.

The theoretical and measured density was 7.21 and 6.675 respectively. From these value we note that the theoretical density has value is larger than the value of the measured density, this may be attributed to the presence of porosity in samples. The porosity of the sample can be calculated from the relation [23]

Porosity % = [(theoretical density - measured density)/(theoretical density)] x 100

In addition, Porosity equal 7.42%.

The variations of real part (έ) of dielectric constant and loss tangent (tan δ) with temperature at various frequencies is shown in figure 1 shows. It is evident from this figure that the phase transition is very diffuse and shows

very strong frequency dispersion at temperatures from room temperature up to 60 ^{o}C. However it does not correspond to a relaxor ferroelectric behavior since the peaks in έ and tan δ occur at the same Curie point which is frequency independent also. For relaxors, the two peak temperatures are non-coincident and both frequency dependent [24-26]. From figure 1 can be noted that the dielectric constant increases with the rise in temperature up to maximum value at Curie temperature and then decreases with further increase in temperature. This is due to the presence of space charge polarization in the materials [27]. Also note the maximum peak of dielectric constant independent on the frequency of the field and it does coincide with the peak of the loss tangent, it's corresponding to the behavior of normal ferroelectric. However, it does not correspond to a relaxor ferroelectric behavior since the peaks in έ and tan δ occur at the same Curie point. For reloxors, the two peaks temperatures are non-coincident and both are frequency dependent. Thus, the dielectric response shown in figures is due to a non-relaxor type diffuse ferroelectric transition.
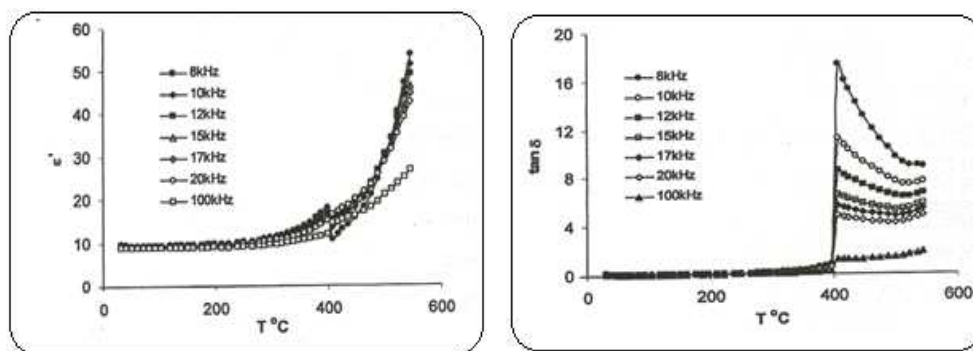

Figure 1: The Variations of Real Part of Dielectric Constant (a) and Loss Tangent (b) with Temperature at Various Frequencies

It's observed that the compounds undergo phase transition from ferroelectric state to paraelectric state at particular temperature called Curie temperature T_c. For a normal ferroelectric, in the vicinity of the T_c (transition temperature), the dielectric stiffness (1/ε), follow the well-known Curie-Weiss law [24].

$$1/\varepsilon = (T - T_o)/C \tag{4}$$

where C is the Curie-Weiss constant and T_o is the Curie-Weiss temperature.

In addition, the order of the ferroelectric to paraelectric phase transition can be determined from the temperature dependence of the dielectric constant inverse (1/ ε). When T_0 is smaller than T_C we observe a first-order transition; on the other hand, when $T_0=T_C$, a second-order transition is observed[28]. The temperature behavior of the inverse of the dielectric constant at different frequencies is shown in figure 2.
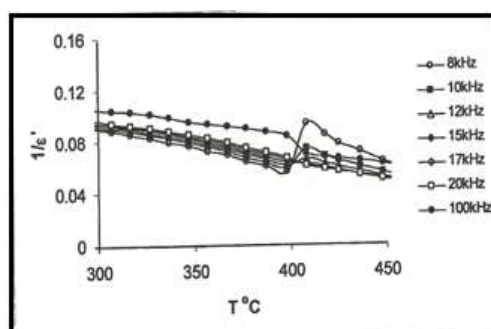

Figure 2: The Inverse of the Dielectric Constant at Different Frequencies

The parameters C and T_o were fitted at a narrow temperature range near T_c, the fitting parameters are $C = 0.05115 \times 10^5$ K and $T_o = 655$ K. The fact that the Curie-Weiss temperature is lower than the transition temperature ($T_c = 671$ K) is expected from the first-order phase transition between the paraelectric and ferroelectric phases.

The measured dielectric constant decreases to rather very low values for frequencies as shown in figure 3 at room temperature. Such a decrease in the value of the dielectric constant at higher frequencies can be explained in terms of the interfacial polarization. Interfacial polarizability results due to the difference in the conductivity of the grains and the grain boundaries. [29]

The higher values of dielectric constant at low frequency suggest the presence of all types of polarization (interfacial, atomic, dipolar, ionic and electronic) at room temperature. At very low frequency, dipoles follow the field and we have high value of dielectric constant. As the frequency increases dipoles begin to lag behind the field and the dielectric constant slightly decreases. Further, at high frequencies dipoles can no longer follow the field and we have low values of dielectric constant. [30] It is known that the dielectric relaxation does depend on the heterogeneity of the samples. Since the materials that are being dealt with in the present investigations are diphasic and heterogeneous in nature, we thought it worth adopting an impedance analysis approach, which is an ideal and powerful tool to probe into details such as bulk and grain boundary effects in ceramics. In the complex impedance plane plots (Cole–Cole) a single semicircle suggests the bulk and a second semicircle suggests the grain boundary effects. Each of the semicircles is represented by a single RC combination. A depressed semicircle, whose center lies below the real axis, suggests a departure from the ideal Debye-like behavior. The inverse peak frequency of the semicircle indicates the relaxation time. The dielectric constant was evaluated using the following relations.
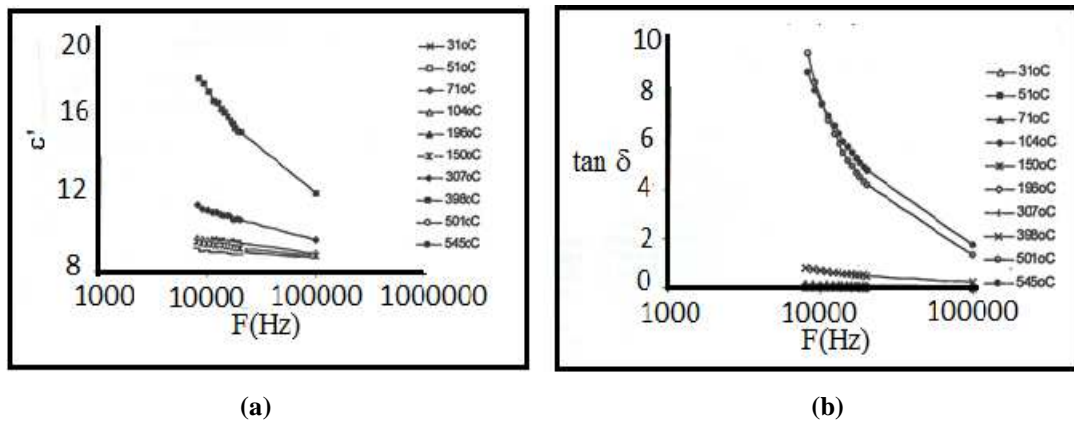

| (a) | (b) |

**Figure 3: The Variations of Real Part of Dielectric Constant with
Various Frequencies at Room Temperature**

$$\varepsilon^{'} = \frac{C_p d}{A \varepsilon_o}$$

(5)

where d is the thickness and A the area of the electrode sample and ε_o is the permittivity of free space.

$$\varepsilon^{''} = \varepsilon^{'} \tan\delta$$

(6)

The measured data (ε' and ε'') are transformed to Z' and Z'' (real and imaginary parts of the impedance) using the following standard relations:

$$Z^* = \frac{1}{j\omega C_o \varepsilon^*}$$ (7)

$$Z' = \frac{\varepsilon''}{\omega C_o \left(\varepsilon'^2 + \varepsilon''^2\right)}$$ (8)

$$Z'' = \frac{\varepsilon'}{\omega C_o \left(\varepsilon'^2 + \varepsilon''^2\right)}$$ (9)

where ω the angular frequency, $\omega = 2\pi f$, C_o is the vacuum capacitance (ε_o A/d). The frequency dependent properties of materials can be described via the complex permittivity (ε^*)($\varepsilon^* = \varepsilon` - i\,\varepsilon``$) $i$ is the complex number, Complex impedance (Z*) ($Z^* = Z` - i\,Z``$) and dielectric loss or dissipation factor ($\tan\delta$) [31]. The results are presented in the complex impedance plane in which Z'' versus Z' are plotted on a linear scale. The value of the bulk resistance (R_b) is found by the low frequency intercept of the semicircle on the real axis (x-axis). The semicircle passes through a maximum at a frequency f_o (relaxation frequency) and satisfies the condition.

$$2\mathrm{p}f_o\, R_b C_b \sim 1$$ (10)

From the above equation the value of bulk capacitance (C_b) is evaluated [26]. One of the advantages of frequency dependent measurements is that the contributions of the bulk materials, the grain boundaries and electrode effects can easily be separated if the time constants are different enough to allow separation. The frequency dependence of Z' and Z'' are plotted for different temperatures of PbTiO$_3$ is shown in figure 4.
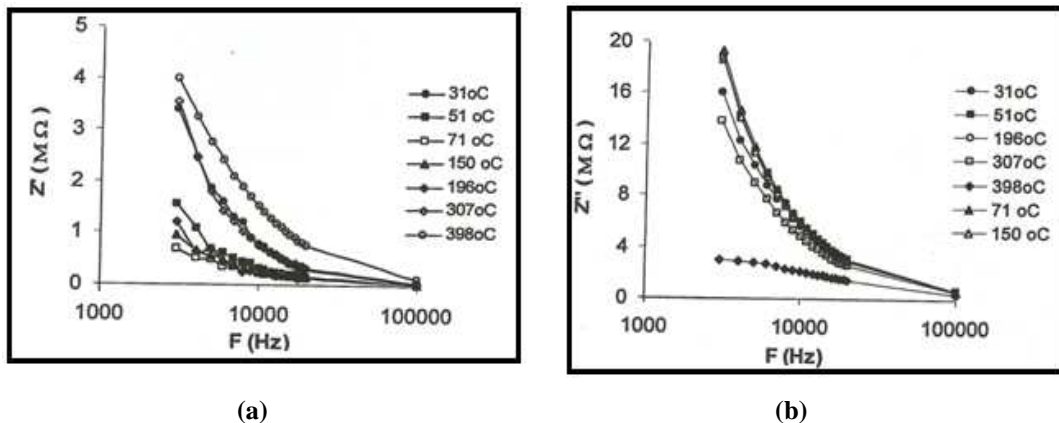

(a)   (b)

Figure 4: The Variation of Z' as a Function of Frequencies at Various Temperature

Figure 5 shows the variation of Z' as a function of temperature at various frequencies for lead titanate. All curves present two peaks the first peak at 100 ^{o}C for all frequencies, which also resembles with the dielectric data at figure 1. The second peak at 313 ^{o}C at 1 kHz and shift to higher temperature side as frequency increases. This indicates that the relaxation process in the sample [32].
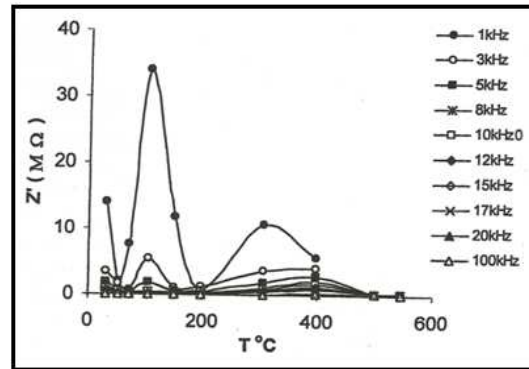
Figure 5: The Variation of Z' as a Function of Temperature at Various Frequencies

Complex impedance spectrum (Nyquist plots i.e. Z" vs. Z') at different temperatures for lead titante is shown in figure 6.
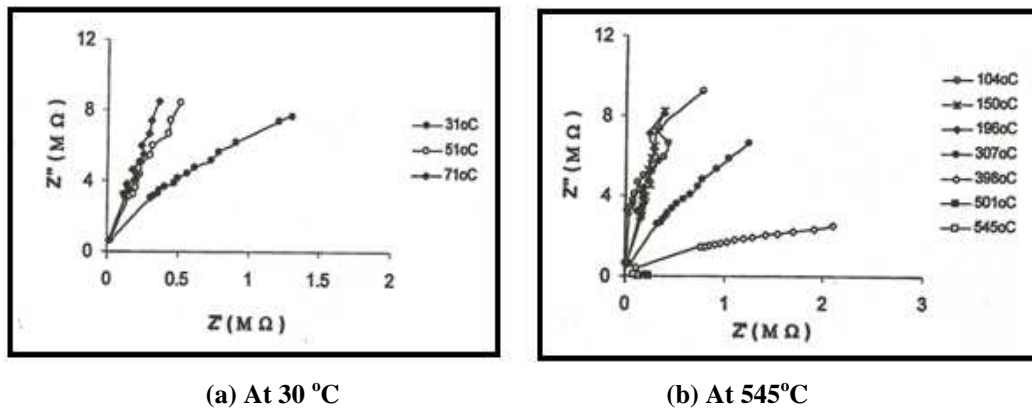

|(a) At 30 ^{o}C | (b) At 545°C|

Figure 6: The Relation between Z" and Z' at Different Temperatures

The impedance plots of the sample were found to exhibit good semicircles. In this sample, only one semicircle has been observed over the entire range of temperature studied. The single semicircles correspond to grains contribution. Some of the impedance data do not take the shape of semicircle in the Nyquist plots rather presents a straight line with large slope, suggesting the insulating behavior of the materials. At definite temperature the slope of the lines decreases and they curved towards real Z' axis and could be traced, indicating increase in the conductivity of the sample. The inspection of the semicircle showed that there is a depression angle instead of a semicircle centered on the real axis.
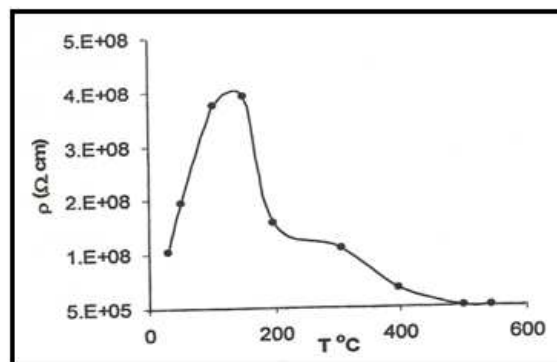

**Figure 7: The Variation of D.C. Resistivity Obtained from
Nyquist Plots as a Function of Temperature**

From figure 7 we note that, above Curie temperature until 150 ^{o}C the material has dρ/dT > 0 (+ temperature coefficient), and the material behave as a metal. After this temperature the material has dρ/dT < 0 (- negative temperature coefficient) and material behave as a semiconductor. Also we note that the sintered ceramics exhibits an anomalous rise in the resistivity by one order of magnitude for this sample after Curie temperature. This phenomenon is commonly known as positive temperature coefficient of resistivity effect, which is widely associated to a grain boundary region, this region leads to high resistivity of the ceramic material above T_c. In the ferroelectric phase the spontaneous polarization results in compensation of surface states.

The PTCR effect is observed from the transition temperature of the ceramic until the temperature of higher value of resistivity. In that temperature range, the grain-boundaries do not show an important contribution to the AC sample response, which is associated to the high bulk resistivity. The grain boundary contribution could be treated as separate or partly resolved second semicircle in the complex plane plots depending on the relative magnitudes of the resistivity for the bulk and grain boundary, which depends on the grain size. The grain size and the homogeneous grain structure could limit the grain boundary contribution in the complex impedance plane [33]. The sample has been prepared taking into account a cationic vacancy [34]. The Arrhenius behavior of the bulk resistivity in a wide temperature range above the Curie point for this sample is shown in figure 8.

Figure 8 shows activation energy value about 0.02 eV which could be associated to an oxygen vacancies movement. It has been known that virtually there is no ionic transport in the perovskite lattice due to the low mobility of the cation vacancies. Therefore the oxygen ions make a certain motion in perovskite ceramics [35]. On the other hand, following the Jonker's model [36], it can be showed that a barrier height, B, that varies linearly with temperature, T, and resistivity, ρ.
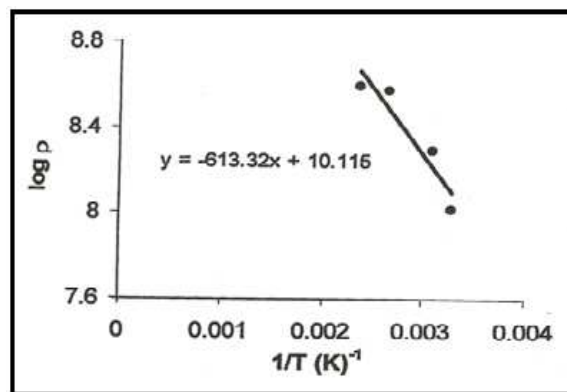

y = -613.32x + 10.115

Figure 8: The Relation between Log ρ and 1/T

If B=B_o (T-T_c), where B_o is a constant, then $\dfrac{d(\log(\rho))}{d(1/kT)} = B_o T_c$. Thus the Arrhenius resistivity above the Curie temperature is predicted by the Jonker's model.

Temperature dependence of the AC conductivity for PbTiO3 at different frequencies is shown in figure 9. From the figure can be note that the conductivity increase with temperature up to 400 ^{o}C and conductivity jump with order equal 1000 times and it increase with further increase of temperature.
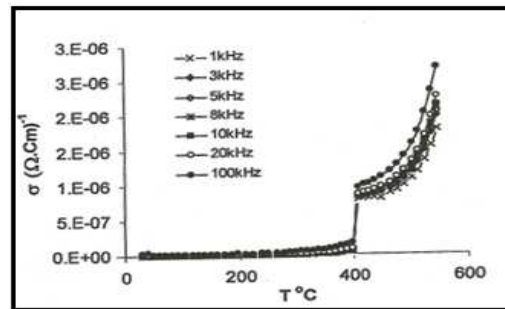
Figure 9: Temperature Dependence of the AC Conductivity at Different Frequencies

Figure 10 shows SEM micrographs for lead titanate. From the figure can note that showed uniform grain distribution on the surface of the samples. Also found the grain size from SEM which equal 3.06 μm.
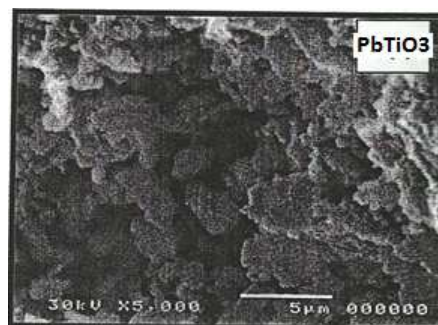

Figure 10: Shows SEM Micrographs for Lead Titanate

From equation 7, can calculate the equivalent circuit for the sample as shown in figure 11. Where $R_b = 80$ MΩ, $C_b = 0.004$ nF.
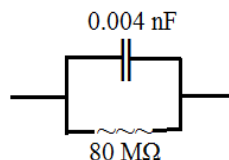

Figure 11: The Equivalent Circuit for the Sample

CONCLUSIONS

Lead titanate, $PbTiO_3$ nano-crystallite was produced (≈ 60 nm) using the solid-state reaction method. The AC behavior of the nano-crystallite PT ceramic sample was studied in wide temperature range from room temperature (18 ^{o}C) to 500 ^{o}C and frequency from 100 Hz to 100 KHz. The results show diffuse phase transition and high dielectric constant at lower frequencies. A PTCR was observed in the temperature dependence of the ceramic resistivity. The results are explained on the basis of the Heywang and Jonker models. The Schottky barrier formed at grain boundary regions act as traps of the electrons available from oxygen vacancies in the ceramics. This provides positive temperature coefficient of resistivity characteristics from the transition temperature to about 210°C.

REFERENCES

1. Y. Xu, (1991) 'Ferroelectric Materials and their Applications', Elsevier Science Publishers B.V., the Netherlands.

2. G.A. Rossetti, L.E. Cross, J.P. Cline, (1995) J. Math. Sci. 30, 24.

3. H. Ihrig, W. Puschert, (1977) A systematic experimental and theoretical investigation of the grain-boundary resistivities of *n*-doped $BaTiO_3$ ceramics, J. Appl. Phys. 48 (7) 308.

4. H.-Y. Chang, K.-S. Liu, I. Nan Lin, (1996) Modification of PTCR behavior of $(Sr_{0.2}Ba_{0.8})$ TiO_3 materials by post-heat treatment after microwave sintering, J. Eur. Ceram. Soc. 16, 63.

5. D.C. Sinclair, A.R. West, (1989), Impedance and modulus spectroscopy of semiconducting $BaTiO_3$ showing positive temperature coefficient of resistance, J. Appl. Phys. 66 (8) 3850.

6. A. Pelaiz-Barranco, I. Gonzalez-Carmenate, F. Calderon-Pinar, E. Torres-Garcia, (2004), AC behavior and PTCR effect in PZN-PT-BT ferroelectric ceramics, Solid State Communication 132 431-435.

7. O. I. Prokopla, I. P. Reavskii, E. I. Bondarenko, A. N. Palvov, (1984) Preparation and study of $KNbO_3$ PTC ceramics, Ferroelectr. Lett. Sect., 2, 1.

8. I. P. Reavskii, A. N. Palvov, O. I. Prokopla, E. I. Bondarenko, (1988) The ptc effect in oxides of the perovskite family, Ferroelectric 83, 171.

9. O. Saburi, (1961) Semiconducting bodies in the family of barium titanates, J. Am. Ceram. Soc. 44, 54–63.

10. W. Heywang, (1971) Semiconducting barium titanate, J. Mater. Sci. 6, 1214–1226.

11. G.H. Jonker, (1964) Some aspects of semiconducting barium titanate, Solid State Electron. 7, 895–903.

12. J. Daniels, K.H. Hardtl, R. Wernike, (1978/79) The PTC effect of barium titanate, Philips Tech. Rev. 38, 73–82.

13. W. Heywang, (1964) Resistivity anomaly in doped barium titanate, J. Am. Ceram. Soc. 47, 484–490.

14. M. Kuwabara (1981), Effect of microstructure on the PTCR effect in semiconducting barium titanate ceramics, J. Am. Ceram. Soc. 64, 639–644.

15. M. Kuwabara, (1981) Influence of stoichiometry on the PTCR effect in porous barium titanate ceramics, J. Am. Ceram. Soc. 64, C170–C171.

16. S.-M. Su, L.-Y. Zhang, H.-T. Sun, X. Yao, (1994) Preparation of porous BaTiO3 PTC thermistors by adding graphite porosifiers, J. Am. Ceram. Soc. 77, 2154–2156.

17. T.R. Shrout, D. Moffatt, W. Huebner, (1991) Composite PTCR thermistors utilizing conducting borides, silicides, and carbide powders, J. Mater. Sci. 26, 145–154.

18. J.-G. Kim, W.-S. Cho, K. Park, (2000) PTCR characteristics in porous (Ba,Sr)-TiO3 ceramics produced by adding partially oxidized Ti powders, Mater. Sci. Eng. B 77, 255–260.

19. T. Takahashi, Y. Nakano, N. Ichinose, (1990) Influence of reoxidation on PTC effect of porous BaTiO3, J. Ceram. Soc. Jpn. 98, 879–884.

20. Software for automated powder diffraction fifth edition, February 1994.

21. Warren B. E., (1969) "X-ray diffraction" Addison-Wesley: Reading, Mass.

22. C.N. Chinnasamy, B. Jeyadevan, K. Shinoda, K. Tohji, D.J. Djayaprawira, M. Takahashi, R. Justinand, A. Narayanasamy, (2003) Appl. Phys. Lett. 83 (14), 2862.

23. Banarji Behera, P. Nayak, R. N. P. Choudhary, (2008) Materials Research Bulletin 43, 401-410.

24. F.M.Pontes, D.S.L.Pontes, E.R.Leite, E.Longo A. J. Chiquito, P. S. Pizani, J. A. Varela, (2003) Electrical conduction mechanism and phase transition studies using dielectric properties and Raman spectroscopy in ferroelectric Pb0.76Ca0.24TiO3 thin films, J. App. Phy., 94, 11, 7256.

25. K. Prasad, Lily, K. Kumari, K.L. Yadav, (2007) Hopping type of conduction in (Na0.5Bi0.5)ZrO3 ceramic, Journal of Physics and Chemistry of Solids 68, 1508–1514.

26. G. Senthil Murugan and K. B. R. Varma, (2002) Lithium borate–strontium bismuth tantalate glass nanocomposite: a novel material for nonlinear optic and ferroelectric applications, J. Mater. Chem., 12, 1426 – 1436.

27. Banarji Behera, P. Nayak, R.N.P. Choudhary, (2008) Structural and impedance properties of $KBa_2V_5O_{15}$ ceramics Materials Research Bulletin 43, 401–410.

28. J. Ravez, C. Brouster, A. Simon, (1999). Lead-free ferroelectric relaxor ceramics in the $BaTiO_3$-$BaZrO_3$-$CaTiO_3$ system J. Mater. Chem. **9**, 1609.

29. Satendra Pal Singh, Akhilesh Kumar Singh, Dhananjai Pandey (2005) Barrier Layer Formation and PTCR Effect in (1 - x) $[Pb(Fe_{1/2}Nb_{1/2})O_3]$-$xPbTiO_3$(x= 0.13) Ceramics, Ferroelectrics 324, 49-53.

30. F. M. Pontes, S. H. Leal, E. R. Leite, E. Longo P. S. Pizani, A. J. Chiquito, J. A. Varela, (2004) Investigation of phase transition in ferroelectric $Pb_{0.70}Sr_{0.30}TiO_3$ thin films, J. Appl. Phys. **96**, 1192.

31. M. Pastor, (2008) Synthesis, structural, dielectric and electrical impedance study of $Pb(Cu_{1/3}Nb_{2/3})O_3$, Journal of Alloys and Compounds 463, 323-327.

32. C K SUMAN, K PRASAD, R N P CHOUDHARY, (2004) Impedance analysis of $Pb_2Sb_3LaTi_5O_{18}$ ceramic Bull. Mater. Sci., 27, 6, 547-553.

33. Huiming GU, Wan Y. Shih, Wei-Heng Shih, (2003) Single-Calcination Synthesis of Pyrochlore-Free $0.9Pb(Mg_{1/3}Nb_{2/3})O_3$–$0.1PbTiO_3$ and $Pb(Mg_{1/3}Nb_{2/3})O_3$ Ceramics Using a Coating Method, Journal of the American Ceramic Society 86[2], 217-221.

34. A. PelaÂ iz Barranco, F. CalderoÂ n PinÄ ar, O. PeÂrez MartõÂnezy, J. De Los Santos Guerra, I. GonzaÂ lez Carmenate (1999) AC Behaviour and Conductive Mechanisms of 2.5 mol% La_2O_3 Doped PbZr $_{0.53}$Ti $_{0.47}O_3$ Ferroelectric Ceramics Journal of the European Ceramic Society 19, 2677-2683.

35. A. Peláiz-Barranco, Y. González-Abreu, (2009) Oxygen vacancies related electrical response in modified lead titanate ceramics, Solid State Communications.

36. Chun-Hung Lai, Chen-Tsang Weng, Tseung-Yuen Tseng, (1995) The effects of Nd_2O_3 additives and Al_2O_3---SiO_2---TiO_2 sintering aids on the electrical resistivity of $(Ba,Sr)TiO_3$ PTCR ceramics, Materials Chemistry and Physics 40, 168-172.